Reference: *Biol. Bull.* **200:** 9–19. (February 2001)

Three-Dimensional Analysis of Finlet Kinematics in the Chub Mackerel (*Scomber japonicus*)

JENNIFER C. NAUEN* AND GEORGE V. LAUDER

Department of Organismic and Evolutionary Biology, Harvard University, 26 Oxford Street, Cambridge, Massachusetts 02138

Abstract. Finlets, which are small non-retractable fins located on the body margins between the second dorsal and anal fins and the caudal fin of scombrid fishes, have been hypothesized to improve swimming performance. The kinematics of three posterior finlets of the chub mackerel, *Scomber japonicus,* were examined using three-dimensional measurement techniques to test hypotheses on finlet rigidity and function during steady swimming. Finlet bending and finlet planar orientation to the *xz*, *yz*, and *xy* planes were measured during steady swimming at 1.2 lengths s^{-1} in a flow tank.

Despite very similar morphology among the individual finlets, there was considerable variability in finlet flexure during a stroke. Several of the finlets were relatively rigid and flat (with intrafinlet angles close to 180° during the stroke), although intrafinlet angle of the proximal portion of the most posterior finlet varied considerably over the stroke and was as low as 140° midstroke. Finlets showed complex orientations in three-dimensional space over a stroke, and these orientations differed among the finlets. For example, during tail deceleration the proximal portion of the fifth finlet achieves a mean angle of approximately 75° with the *xz* plane, while the distal portion of this finlet is oriented at 110°. Our data suggest that the trajectory of local water flow varies among finlets and that the most posterior finlet is oriented to redirect flow into the developing tail vortex, which may increase thrust produced by the tail of swimming mackerel.

Received 30 May 2000; accepted 1 December 2000.

* To whom correspondence should be addressed. E-mail: jnauen@oeb.harvard.edu.

Introduction

Finlets are small non-retractable fins characteristic of scombrid fishes including mackerel, bonitos, and tuna (Collette and Nauen, 1983; Joseph *et al.,* 1988). The finlets are situated on the dorsal and ventral body margins adjacent to the tail (spanning the region between the second dorsal and anal fins and the caudal fin, Fig. 1). In the case of the five dorsal and five ventral finlets of the chub mackerel, *Scomber japonicus* (Fig. 1), the summed surface area of the finlets is about 15% of the surface area of the caudal fin (Nauen and Lauder, 2000). Muscles that may actively control finlet motion insert at the base of each finlet (Nauen and Lauder, 2000).

Scombrid fishes are capable of high locomotory performance, including burst speeds from 18 body lengths per second ($bl\ s^{-1}$) for mackerel (Wardle and He, 1988) to up to 27 $bl\ s^{-1}$ for tuna (Fierstine and Walters, 1968; also see Magnuson, 1978), and cruising speeds from 3.5 $bl\ s^{-1}$ for mackerel (Wardle and He, 1988) to 6–10 $bl\ s^{-1}$ for tuna (Yuen, 1970; summarized in Beamish, 1978). Given the close proximity of finlets to the caudal fin, previous investigators have suggested that finlets play a role in locomotion. Walters (1962) proposed that finlets direct flow longitudinally along the body, and Magnuson (1970) and Lindsey (1978) suggested that finlets direct flow across the caudal peduncle and caudal keels.

A recent study by Nauen and Lauder (2000) using two-dimensional (2-D) kinematic analysis methods to quantify the kinematics of finlets of *S. japonicus* showed that during steady forward locomotion at speeds from 1.2 to 3.0 fork lengths (l) s^{-1}, finlet kinematics in the vertical (xy) and horizontal (xz) plane were independent of speed. Angle of attack calculations using the kinematic measurements and the assumption that the direction of flow incident to the finlet was equal and opposite to the path of motion of the

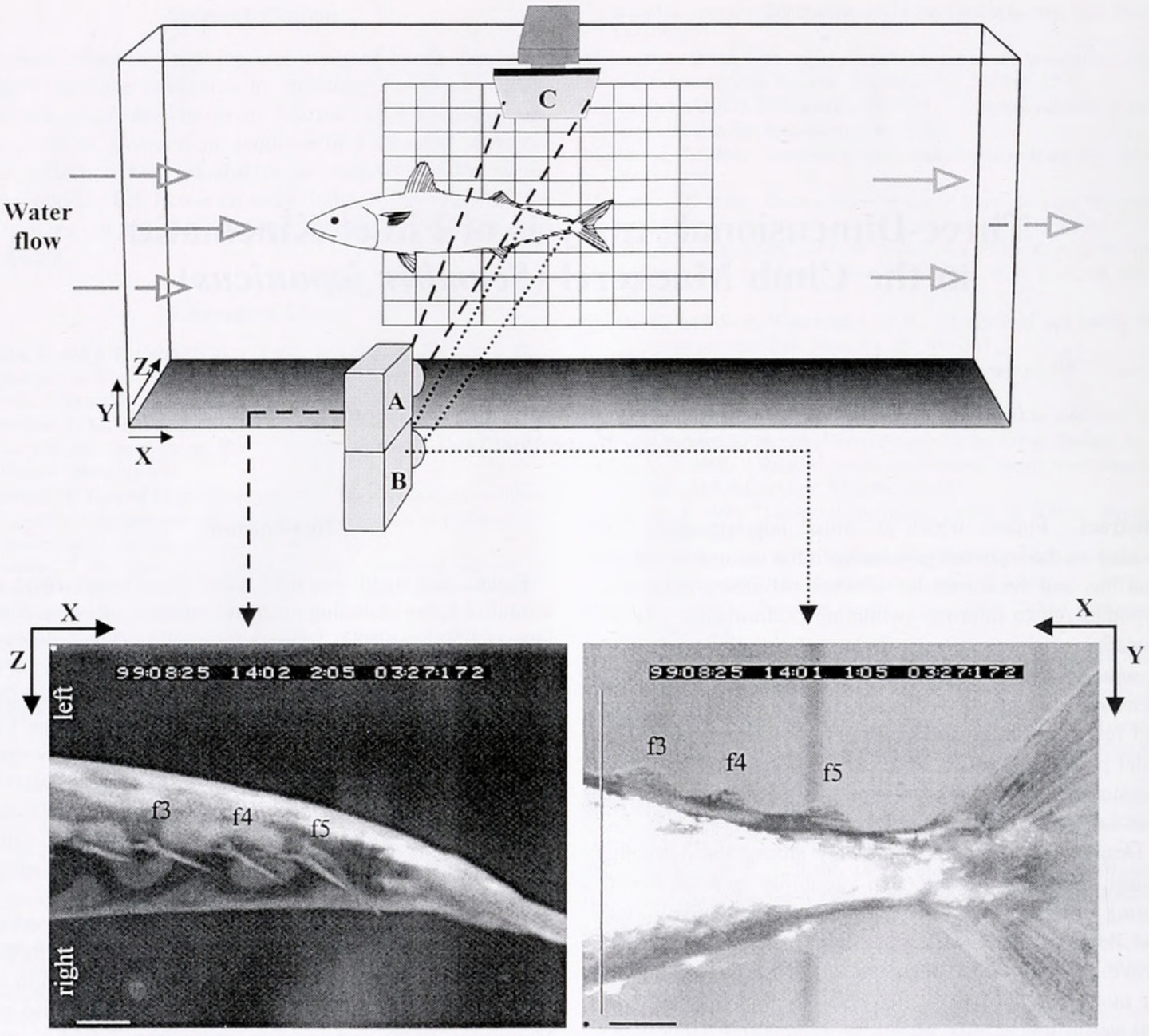

Figure 1. A schematic of the flow tank and camera system showing camera A (dashed line) viewing the mirror (C), which was situated at a 45° angle to the *xz* plane and showed a dorsal view of the fish. The origin of the dorsal view image (white asterisk in the left image) was in the upper left corner of the image. The viewing area of camera B (dotted line) was a lateral view of the left side of the fish; the origin of the lateral image (black asterisk in the right image) was in the lower left corner of the image. The three posterior finlets are identified in both of the images. Scale bars indicate 1 cm.

fish indicated that finlet oscillation in the horizontal plane is largely passive, and thrust is not created by lift-based mechanisms. However, the position of the finlets as the tail decelerates (at the end of each stroke) suggests that the finlets might direct flow into the developing caudal fin vortex, thus enhancing vortex circulation and thrust.

The 2-D method was useful for determining basic patterns of finlet movement and the independence of these patterns from swimming speed (Nauen and Lauder, 2000). A limitation of this method, however, was that each finlet was considered to be a flat plate that acted as a single functional unit during the tail beat cycle. Thus, any flexion of the finlet in response to hydrodynamic load was neglected. Furthermore, the orientations of the finlets in three-dimensional (3-D) space were not determined. This information is important for understanding finlet hydrodynamic function because it is the motion and orientation of the surface of a fin that creates fluid motion and generates force (Dickinson, 1996). For examples of how 2-D kinematic measurements can be misleading for evaluating fin hydrodynamics, see Ferry and Lauder (1996), Lauder and Jayne (1996), Walker and Westneat,

(1997), Gibb *et al.* (1999), Wilga and Lauder (1999), and Lauder (2000).

Thus, the primary goal of this paper is to quantify the movement of finlets in three dimensions and to describe the orientation of the finlet surfaces with respect to three external earth reference planes (*xy*, *xz*, and *yz*). To test the hypothesis that each finlet acts as a single rigid flat plate, we divided each finlet into two separate elements and calculated the internal angle of these elements to each other as an approximation of finlet curvature. *A priori* we expected that finlet deformation would be low, because a dense assembly of fin rays support each finlet (Nauen and Lauder, 2000), and that the magnitude of flexion and 3-D orientation of the finlets would be similar, because the individual finlets are very similar in morphology (see Fig. 1, Fig. 2, and Nauen and Lauder, 2000). Using the 3-D data, we determined the position of the finlets during a critical portion of the stroke cycle when, as predicted by the vorticity enhancement hypothesis described above, the finlets may redirect water flow towards the caudal fin vortex. We then use these data to predict the direction of water motion in the region of the finlets.

Materials and Methods

Animals

Chub mackerel, *Scomber japonicus* (Houttuyn) were collected, using rod and reel, from various locations in coastal southern California. The animals were fed chopped smelt and housed in 1200-l tanks at a water temperature of 18 ± 2 °C in a photoperiod of 12:12 h light:dark. Three individuals (numbered 7, 9, and 10) ranging in fork length (l) from 20 to 26 cm were studied here.

3-D kinematic measurements

Experiments were conducted using a 600-l flow tank with a working area 82 cm long × 28 cm wide × 28 cm high (Fig. 1) and a water temperature of 19 ± 1 °C. The speed profile of the flow across and along the working section of the tank has been determined by tracking dye streams on images collected using high-speed video (for details, see Jayne *et al.*, 1996). To accurately image the motion of the finlets for a series of tailbeats, it was necessary that the fish maintain a consistent position relative to the field of view of the cameras. Thus, we used a flow tank rather than have the fish swim in still water through the field of view.

Two cameras that were part of a NAC HSV 500 C^3 video system were mounted on a vertical frame and aimed perpendicular to the flow tank (Fig. 1). The upper camera (Fig. 1A) was focused on a front-surface mirror (Fig. 1C) that was immersed in the flow at a 45° angle to the bottom of the tank (the *xz* plane) and showed a dorsal view of the fish. The lower camera (Fig. 1B) provided a lateral view (the *xy* plane) of the finlets. Using Nikon Micro-Nikkor 55-mm lenses with these cameras, we were able to image the finlets clearly in a field of view that was about 5 cm × 4 cm (Fig. 1). When a mackerel was in the field of view of the cameras and the image was in focus, the animal was necessarily swimming in the center of the working section of the tank. Thus, no data were obtained near the walls or floor of the flow tank, or the upper surface of the water. The fields of view of both cameras were scaled at the start of the experiment using two perpendicularly oriented rulers. The video system electronically synchronized the two cameras and recorded images at 250 Hz. About 12–15 images were collected per stroke of the tail. Video images were recorded continuously until sufficient sequences of steady swimming with the finlets in the fields of view of both cameras were obtained.

We swam the mackerel at speeds of 1.2 and 2.2 fork lengths per second ($l\ s^{-1}$). These speeds are within the range of swimming speeds (0.4–3.5 $bl\ s^{-1}$) that mackerel can sustain for longer than 200 min (Wardle and He, 1988), and match the speeds used in previous kinematic studies of mackerel finlets (Nauen and Lauder, 2000) and tail (Gibb *et al.*, 1999).

The video images were imported into a computer using DT-Acquire software with a Data Translation video card (Data Translation, Inc.). The procedures for calculating 3-D kinematics were adopted from those used in previous studies (Lauder and Jayne, 1996; Wilga and Lauder, 1999; Lauder, 2000). With the Cartesian coordinate system, any point on the video images can be identified by *x*, *y*, and *z* values. The origin was assigned to the lower left corner of the lateral view and the upper left corner of the dorsal view because the dorsal view was recorded using a mirror (the origin is denoted by asterisks in the images in Fig. 1). Because the finlets move over the body midline with each stroke (Nauen and Lauder, 2000), and we viewed the left side of the fish, the finlets were in full view of camera B as the tail was beating from left to right. There is a phase lag in the movement of the finlets relative to the body (Nauen and Lauder, 2000), thus the finlets are in view from about the start of the second quarter of one stroke to the end of the first quarter of the next (as determined by digitizing the dorsal insertion of finlet 5A, see Figs. 3 and 5).

The movements of finlets 3, 4, 5A, and 5B were quantified in this study. Previous kinematic measurements (Nauen and Lauder, 2000) indicated that finlet size and amplitude of finlet movement decrease anteriorly, with finlets 1 and 2 showing small excursions compared to those of finlet 5. In addition, the body of *S. japonicus* tapers posteriorly (Fig. 1). For example, for the fish 23 cm in fork length examined here, the depth of the body at the insertion of finlet 5 was 0.72 cm, which is 30% of the depth of the body at the position of finlet 1. The posterior decrease in the depth of the body and increase in the size and excursion of the finlets result in the posterior finlets moving

over a much greater area of the body. The tips of dorsal and ventral finlet 5B actually meet at the lateral midline of the body on the caudal peduncle during their maximum vertical excursion (see fig. 12 of Nauen and Lauder, 2000). Thus, because the posterior finlets have a much larger potential hydrodynamic effect than the anterior finlets, we quantified the 3-D kinematics of finlets 3, 4, and 5.

The fifth finlet in *S. japonicus* is composed of two distinct groups of fin rays joined by a thin, clear membrane (Nauen and Lauder, 2000). Finlet 5 was treated here as two separate elements, 5A and 5B. The geometric relationship between those two elements (the internal angle of finlet 5) was also quantified. Single finlets 3 and 4 were an interesting comparison to the double-finlet structure of finlet 5.

Each finlet was divided into two triangles that were defined by a series of points (Fig. 2). This method gives a very good representation of finlet shape (Fig. 2) and allowed us to estimate finlet curvature by calculating the angle between the two triangular surfaces (angle α in the animal's frame of reference, Fig. 3), given the assumption of spanwise rigidity of the two triangles. Angle α for finlet 5 as a whole was the angle between finlets 5A and 5B (Fig. 2). The angles made by each of the eight triangular surfaces to the three orthogonal planes in the earth frame of reference (xy, xz, and yz) were also determined (Fig. 3).

Downloaded video images were digitized using a customized program. The coordinates were imported into Excel (Microsoft) to calculate the internal angles of the finlets and the angles of the finlet triangles to the three external reference planes. Each calculated angle was verified in a customized 3-D visualization program. All angle measurements were made from the upstream left side of the triangular surface to the plane of interest (Fig. 3). Under this measurement convention, if the left finlet surface was positioned to the right of the body midline (as shown in Fig. 3) the yz angle was less than 90°; a yz angle greater than 90° indicated that the left finlet surface was on the left side of the body midline. An xz measurement greater than 90° indicated that the surface was tilted away from the floor of the tank (or the frontal plane of the fish, Fig. 3). An xy angle measurement less than 90° indicated that the surface was oriented to the left of the body midline. Values of xy angles decreased to 0° as the finlet moved parallel to the body midline and then abruptly increased to about 120° as the finlet crossed to the right of the body midline. This abrupt increase (see Fig. 5A) is solely due to the measurement convention and does not reflect a large change in orientation of the finlet.

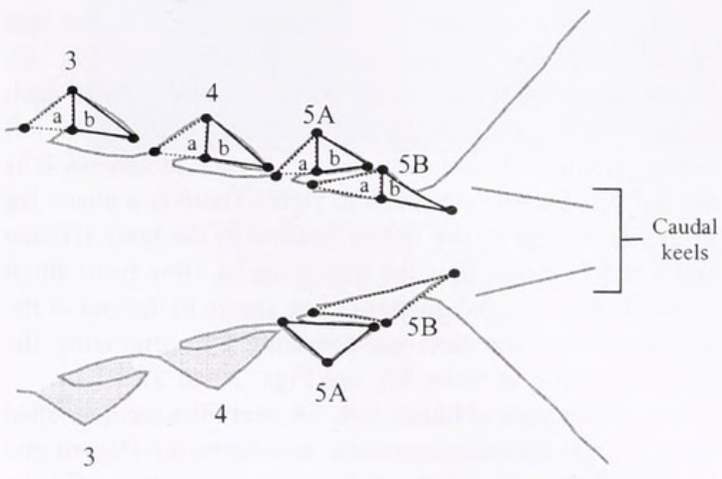

Figure 2. An outline of *Scomber japonicus* (gray lines) traced from a video image showing finlets 3, 4, 5A, 5B, and the caudal keels for reference. Note that the fifth finlet is morphologically composed of two distinct units (5A and 5B) that are bound by a clear membrane (Nauen and Lauder, 2000). Each set of four points (black circles) defined two triangular surfaces shown by the solid and dotted lines. Three of the points on finlets 5A and 5B (illustrated on the ventral finlets for clarity) were used to determine the rigidity of the fifth dorsal finlet as a whole. The thin, clear membrane that covers each of finlets 1–5 and attaches to the body is depicted in gray on ventral finlets 3 and 4.

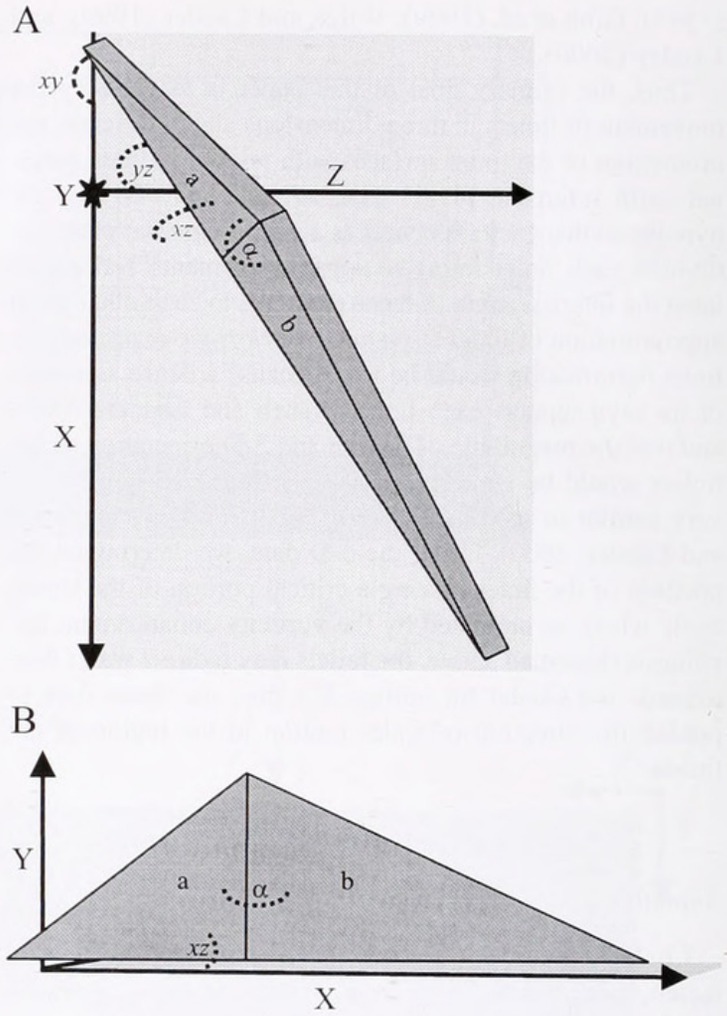

Figure 3. Diagram of a finlet (dark gray triangle) from a dorsal (A) and lateral (B) view. From the dorsal view (A) the y axis (indicated by an asterisk) is coming straight out of the page; in both views the xz plane is light gray. The internal angle (α), and the xy, xz, and yz angles (dotted lines), shown here in the dorsal view of triangle A, were calculated from digitized points (Fig. 2). See the text for further explanation.

Initial comparisons of a time series of the 3-D angles over a complete stroke for a single individual swimming at 1.2 and 2.2 $l\ s^{-1}$ indicated that the general patterns of finlet kinematics were not affected by speed. This observation is supported by our previous finding (based on a statistical analysis of 2-D measurements) that finlet kinematics were independent of speed over a speed range of 1.2 to 3.0 $l\ s^{-1}$ (Nauen and Lauder, 2000). On the basis of this information we focused on the 3-D kinematics of the finlets at the speed of 1.2 $l\ s^{-1}$.

Three to six tail strokes were digitized for each fish. The strokes were from sequential tailbeats for two of the fish; for the third fish we analyzed strokes from two sequential tailbeats and a third, single tailbeat. The digitized position values were not filtered. To determine the digitizing error, we digitized a single finlet 5 times. The calculated angle to the *xy*, *xz*, and *yz* planes were 23.0° ± 0.7°, 91.1° ± 1.0°, and 113.0° ± 0.8° (mean + SD, $n = 5$). Therefore, the digitizing error is approximately 1°. Finlet movement over an entire stroke was determined for one individual; finlet position as the tail was decelerating was determined for multiple strokes from all three individuals.

Statistics

Statistical analyses were performed using Statgraphics (v. 3.0 for Windows, STSC, USA). To determine if the mean values of intrafinlet angles averaged over a tailbeat cycle for a single individual were significantly different from 180°, *t* tests were performed on the time series data. The purpose of this analysis was to determine the general trend of finlet flexibility over the course of a tail stroke. The probability values of the *t* tests were established using the sequential Bonferroni method of Rice (1989) to control for conducting multiple comparisons. A multivariate ANOVA could not be performed on all of the angle data for the multiple individuals because of insufficient degrees of freedom; therefore, the data for each plane (*xy*, *xz*, and *yz*) were separately analyzed using two-way ANOVAS. The position of the finlet on the body (finlet number) was considered a fixed effect, and the individuals were considered random effects. The data at the specific time at 75% of the tail beat cycle—the time when the posterior finlets are in position to influence flow according to the vorticity enhancement hypothesis (Nauen and Lauder, 2000)—were also analyzed using this method. Tukey-Kramer *post hoc* tests were performed on each variable that showed significant effects of speed, finlet number, or structure.

Results

Kinematics over a stroke

Given that the magnitude of digitizing error was about 1° (detailed in the methods section), intrafinlet angle (α) values over a complete stroke for one individual (fish 10) swimming at a slow cruising speed of 1.2 $l\ s^{-1}$ indicate changes in finlet flexure over the stroke and variability in flexure among finlets. The variability in finlet flexibility is not directly attributable to the finlets' position on the body (Fig. 4) given that the greatest difference in α values from 180° (representing a flat plate) were about 40° for finlet 5A and about 15° for finlet 5B, and these two finlets are directly adjacent to each other (Fig. 2). Mean α values over a stroke, which represent a general index of finlet flexion, were not significantly different from 180° for finlets 3 ($\alpha = 179 \pm 6°$, mean ± SD, $n = 11$) and 5B ($\alpha = 182 \pm 10°$, mean ± SD, $n = 10$, *t* test, $P = 0.61$ and 0.52, respectively). The mean α values of finlet 4 (174 ± 6°, mean ± SD, $n = 13$) and finlet 5A (160 ± 18°, mean ± SD, $n = 10$) were significantly different from 180° (*t* test, $P = 0.003$, and 0.006, respectively). The flexion of finlet 5A was largest three-quarters of the way through the stroke (at about 0.75 s in Fig. 4) and decreased to close to zero ($\alpha = 180°$) at the end of the stroke (at about 0.1 s in Fig. 4).

The mean α value of finlet 5 over one stroke for fish 10, measured as the angle between finlet 5A and finlet 5B (see Fig. 2), was significantly different from 180° (*t* test, $P < 0.001$), indicating that the coupling between the two finlets is not rigid. The α for finlet 5 was relatively low throughout the stroke ($\alpha = 157 \pm 8°$, mean ± SD, $n = 10$).

The time series of the orientation of the finlets to the planes *xy* (Fig. 5A, B), *yz* (Fig. 5C, D), and *xz* (Fig. 5E, F) also indicate variability in orientation among the different finlets during different stages in the stroke. The more posterior finlets tended to make greater angles to the *xy* (longitudinal) plane (Fig. 5A, B). The phased increase in *xy* angle to values greater than 90° reflects the finlets crossing the longitudinal body midline to the right side of the fish at the end of the stroke (see Fig. 2). Relative to the *yz* (transverse) plane (Fig. 5C, D), the angles of the finlets decreased throughout the stroke, and were less than 90° for the first quarter of the next stroke. As the *xy* angle increases to greater than 90°, the *yz* angle decreases to less than 90° (Fig. 5A, B), indicating that the finlet has crossed to the right side of the body midline.

The time series of the angle of finlets 3, 4, and 5B to the *xz* plane during a stroke (Fig. 5E, F) suggests that the angles of finlets 3, 4, and 5B were at a slightly obtuse angle to the *xz* plane, while finlet 5A made an acute angle to the *xz* plane. However, when the mean values of the *xz* angle over a stroke were tested using adjusted probability values to control for conducting a series of simultaneous *t* tests (Rice, 1989), this observation was not statistically significant (Table 1). When averaged over an entire tail-beat, the angle of triangles 3A, 3B, 4A, and 4B to the *xz* plane were significantly different from 90° (Table 1), whereas the angles of finlets 5A and 5B were not (Table 1). This surprising statistical result is due to (1) averaging values over the

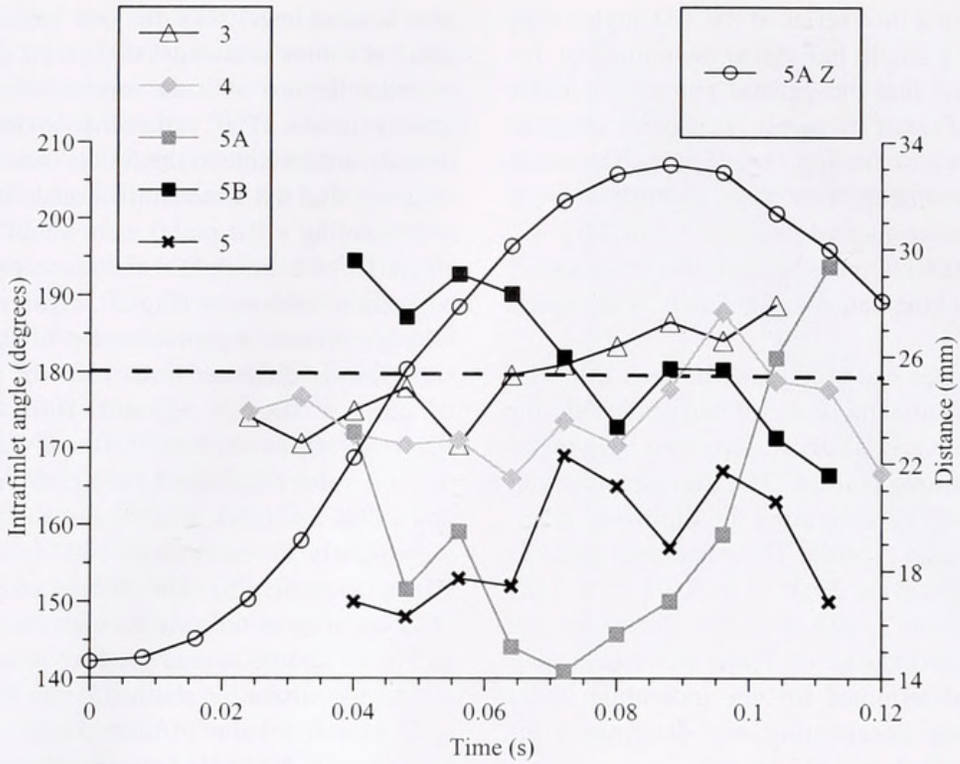

Figure 4. The internal angle (α) of finlets 3 (triangle), 4 (diamond), 5A (gray square), and 5B (black square) of a single individual over a tail stroke at 1.2 $l\ s^{-1}$. The angle between 5A and 5B (crosses) is also plotted. The dashed line indicates 180°. Axial body bending is indicated by the position of the body (at the insertion of finlet 5A) on the z axis (circles, 5A Z).

entire tail stroke and (2) the fact that the P value at which significance is achieved decreases with an increasing number of tests (Rice, 1989). We investigated this further by determining whether the intrafinlet angle differed from 90° at a specific time in the stroke.

Kinematics during tail deceleration

Three-quarters of the way through a stroke, the tail decelerates (Nauen and Lauder, 2000). Intrafinlet angle (α) values averaged from three fish indicate that finlet flexure was low at this point in the stroke, because α values were generally close to 180° (Fig. 6). Individual variation in the α value for finlet 5A was high, however: two of the individuals showed relatively low mean α values (mean ± SD of 151 ± 6° and 153 ± 7°, for fish 10 (n = 6) and fish 9 (n = 3), respectively), similar to the value of 144° seen at that point in the time series of a single stroke for Fish 10 (Fig. 4); in contrast, individual 7 showed a mean α value of 182 ± 1° (n = 3). This variation was reflected in the significant individual effect on α for finlets 4, 5A, 5B, and 5 (F = 15.9, $P < 0.0001$, Table 2). The significant interaction effect (F = 5.4, P = 0.0024, Table 2) indicates that there was no consistent change among individuals in α with position on the body (*i.e.*, finlet number, Fig. 6). There was no significant effect of finlet position on the body on α (F = 3.0, P = 0.16).

At this point in the stroke, the xy angle of the posterior finlets tended to be larger than those of the anterior finlets (Fig. 7A). This difference is reflected in the significant finlet effects (F = 9.2, P = 0.0016, Table 3). There were also significant individual (F = 30.6, $P < 0.0001$, Table 3) and individual × finlet interaction effects (F = 2.98, P = 0.0046, Table 3). The yz angles tended to be greater than 90° (Fig. 7B); the ANOVA indicated significant individual (F = 20.2, $P < 0.0001$) and individual × finlet (F = 9.5, $P < 0.0001$) effects but not significant finlet effects (F = 2.53, P = 0.0996) on the yz angles (Table 3). The xz angles of finlet 5B tended to be greater than 90°, whereas finlet 5A tended to be less than 90° (Fig. 7C). The ANOVA indicated significant finlet (F = 8.12, P = 0.0027, Table 3) and individual × finlet effects (F = 3.64, P = 0.0009, Table 3) but not significant individual effects (F = 1.56, P = 0.2190, Table 3) on the xz angles.

To illustrate the position of the finlets three-quarters of the way through the tail stroke, the coordinates of finlets 4, 5A, and 5B from the time series in Figure 5 are plotted in 3-D space in Figure 8. The data shown here are the highlighted points in the time series (Fig. 5). Although from a lateral view the finlets appear roughly flat and oriented normal to the xz plane (Fig. 8A), the flexure of finlets 4 and 5, the flexure between 5A and 5B, and the acute angle of 5A

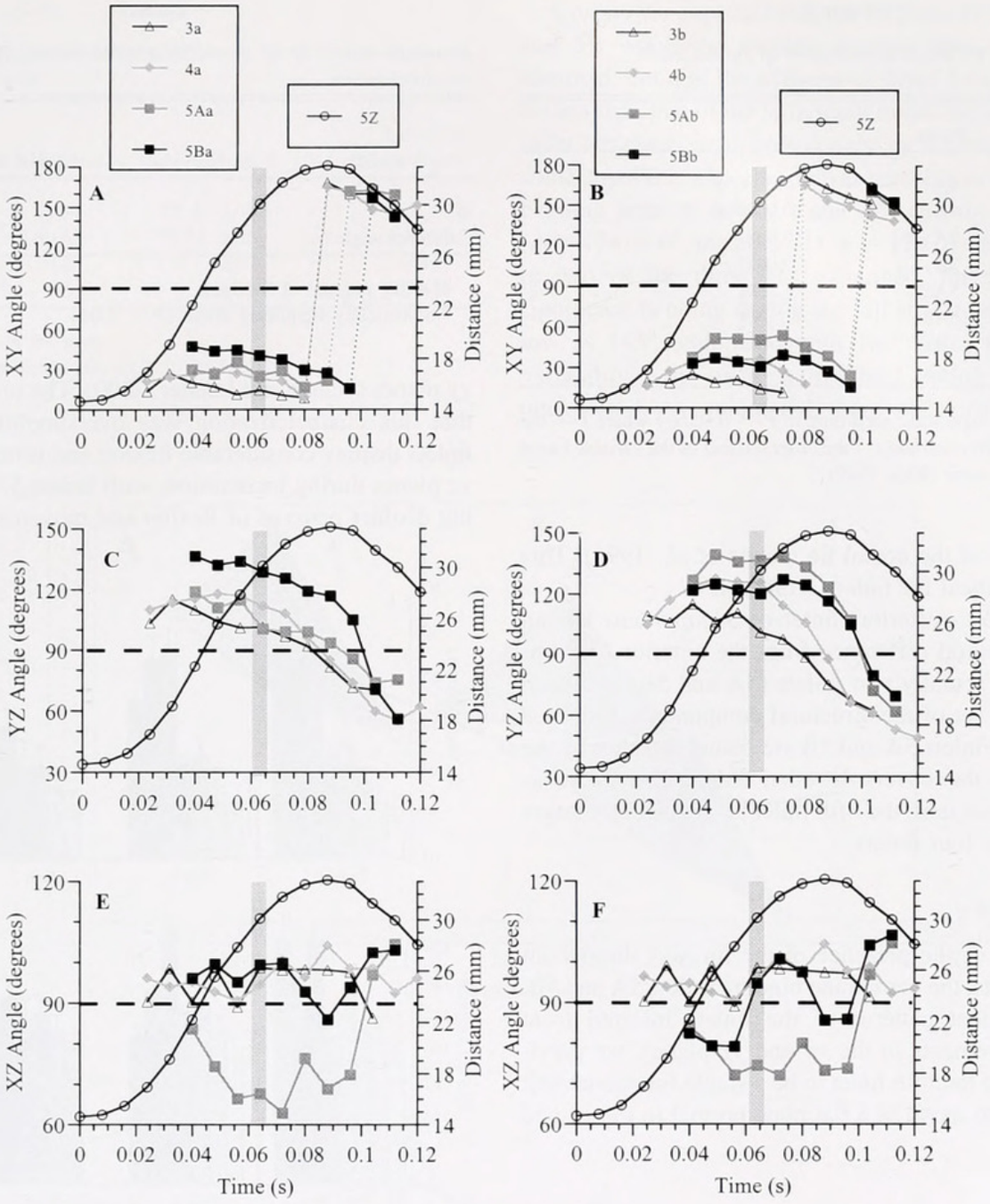

Figure 5. The angle of finlets 3 (triangle), 4 (diamond), 5A (gray square) and 5B (black square) to the *xy* (A, anterior triangles, B, posterior triangles), *yz* (C, D), and *xz* (E, F) planes over a stroke by a single individual at 1.2 $l\ s^{-1}$. Axial body bending is indicated by the position of the body (at the insertion of finlet 5A) on the *z* axis (circles). The tail stroke is defined from minimum to maximum values of 5A Z; the duration of this stroke was approximately 0.09 s. The angles at the time highlighted by the gray bar are plotted in 3-D space in Figure 8. The abrupt change in angles to the *xy* plane in panels A and B (indicated by the dotted lines) is due to our measurement convention (see Fig. 3 and the methods section) and reflects the transition of the planar finlet orientation across the body midline relative to the *xy* reference plane, not a large movement by the finlets.

to the *xz* plane are visible when the lateral view is rotated about 30° clockwise (Fig. 8B).

Discussion

Finlet morphology

A detailed morphological description of the finlets of *Scomber japonicus* is available in Nauen and Lauder (2000), and is useful for interpreting the three-dimensional pattern of movement. In brief, the finlets are on the order of 1 cm in length. A thin, clear membrane covers each finlet and attaches to the body. Jointed bony fin rays that extend to the distal tip of the fin stiffen each finlet. These rays articulate on a cartilaginous pad and are associated with muscles that appear to be homologous to the inclinator, depressor, and

Table 1

Results of t *tests of the angle of each finlet to the* XZ *plane over a stroke*

Finlet	*P*
4A	0.000035
4B	0.000086
3A	0.0087
3B	0.0021
5Aa	NS
5Ab	NS
5Ba	NS
5Bb	NS

NS indicates not significant according to $P = 0.05/k\text{-}i$ where k = the number of t tests performed and i = the order number of the variable based on its calculated P value (Rice, 1989).

Table 2

*Results (*F *values) of the three-way ANOVA on intrafinlet angle during tail deceleration*

Variable	Individual	Finlet #	Individual × finlet
df	2, 27	2, 4	4, 27
Intrafinlet angle (α)	15.9*	3.0	5.4*

df is the degrees of freedom.
* Statistically significant effect ($P < 0.05$).

erector muscles of the dorsal fin (Jayne *et al.*, 1996). This structure is identical for finlets 1 through 4.

The fifth (most posterior) finlet of *S. japonicus* has an interesting structural difference from the anterior four finlets. Finlet 5 is actually two finlets (5A and 5B) that each have a separate set of the structural components described above (Fig. 2). Finlets 5A and 5B are bound together by the clear membrane that covers the other finlets. Considered as a single functional unit, the fifth finlet is significantly larger than the anterior four finlets.

Finlet kinematics

On the basis of the presence of the fin rays throughout each of the finlets, the membrane binding finlets 5A and 5B, and the movement patterns of the finlets inferred from separate measurements in the *xy* and *yz* planes, we previously considered the fifth finlet to be a single functional unit and each finlet to move as a flat plate normal to the *xz* and *xy* planes (Nauen and Lauder, 2000). The present data show that this characterization was oversimplified. All of the finlets display considerable flexion and tilting to the *xz* and *yz* planes during locomotion, with finlets 5A and 5B showing distinct patterns of flexion and movement.

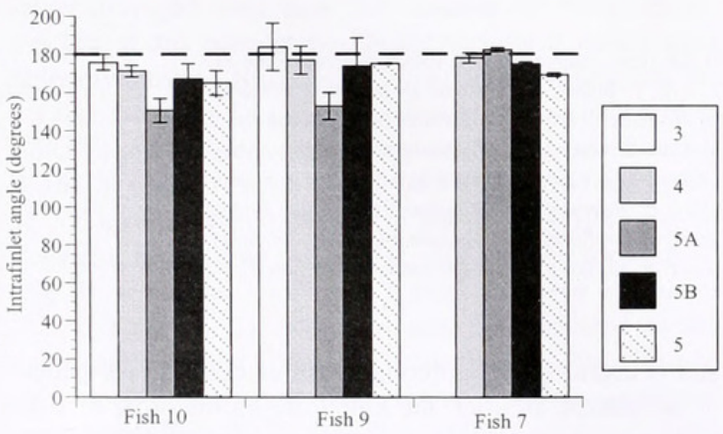

Figure 6. Means and standard deviations of the intrafinlet angle (α) for the finlets of three individuals at a single time point three-quarters of the way through the stroke as the tail is decelerating (n = 6, 3, and 3 strokes for fish 10, 9, and 7, respectively). The dashed line indicates an intrafinlet angle of 180° when the finlet elements are coplanar.

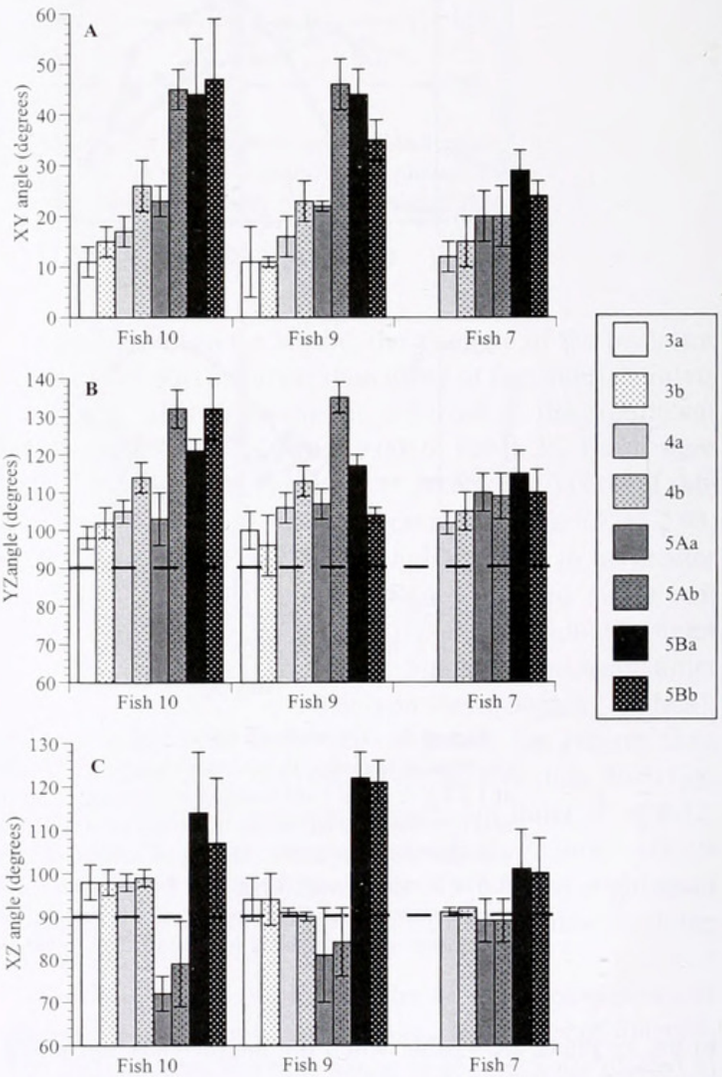

Figure 7. Means and standard deviations of the angles of the anterior (a, solid bars) and the posterior (b, dotted bars) elements of finlets 3 (white), 4 (light gray), 5A (dark gray), and 5B (black) to the three reference planes as the tail is decelerating three-quarters of the way through the stroke (n = 6, 3, and 3 strokes for fish 10, 9, and 7, respectively). The dashed lines in B and C indicate 90°.

Table 3

Results (F values) of the three-way ANOVAs on xy, yz and xz angles during tail deceleration

Variable	Individual	Finlet #	Individual × finlet
df	2, 54	5, 10	10, 54
xy angle	30.6*	9.2*	2.98*
yz angle	20.2*	2.5	9.49*
xz angle	1.6	8.12*	3.64*

df is the degrees of freedom.
* Statistically significant effect ($P < 0.05$).

A priori we expected that the stiffness of finlets 3, 4, 5A, and 5B would be similar because they are structurally identical, but that the stiffness of finlet 5 as a whole would be less than that of the individual finlets because the double-finlet structure is supported only by a clear membrane. In some cases this expectation was corroborated by the lack of bending seen in finlets 3 and 5B, and the slight bending ($\alpha = 174 \pm 6°$, mean $\pm$ SD, $n = 13$) of finlet 4. However, in two of the three fish examined, finlet 5A displayed significant bending during the tail stroke, with α values as low as 145° (compared with 180° for a flat plate). This variability in the stiffness of finlet 5 among individuals was unexpected. As anticipated, there was considerable flexion

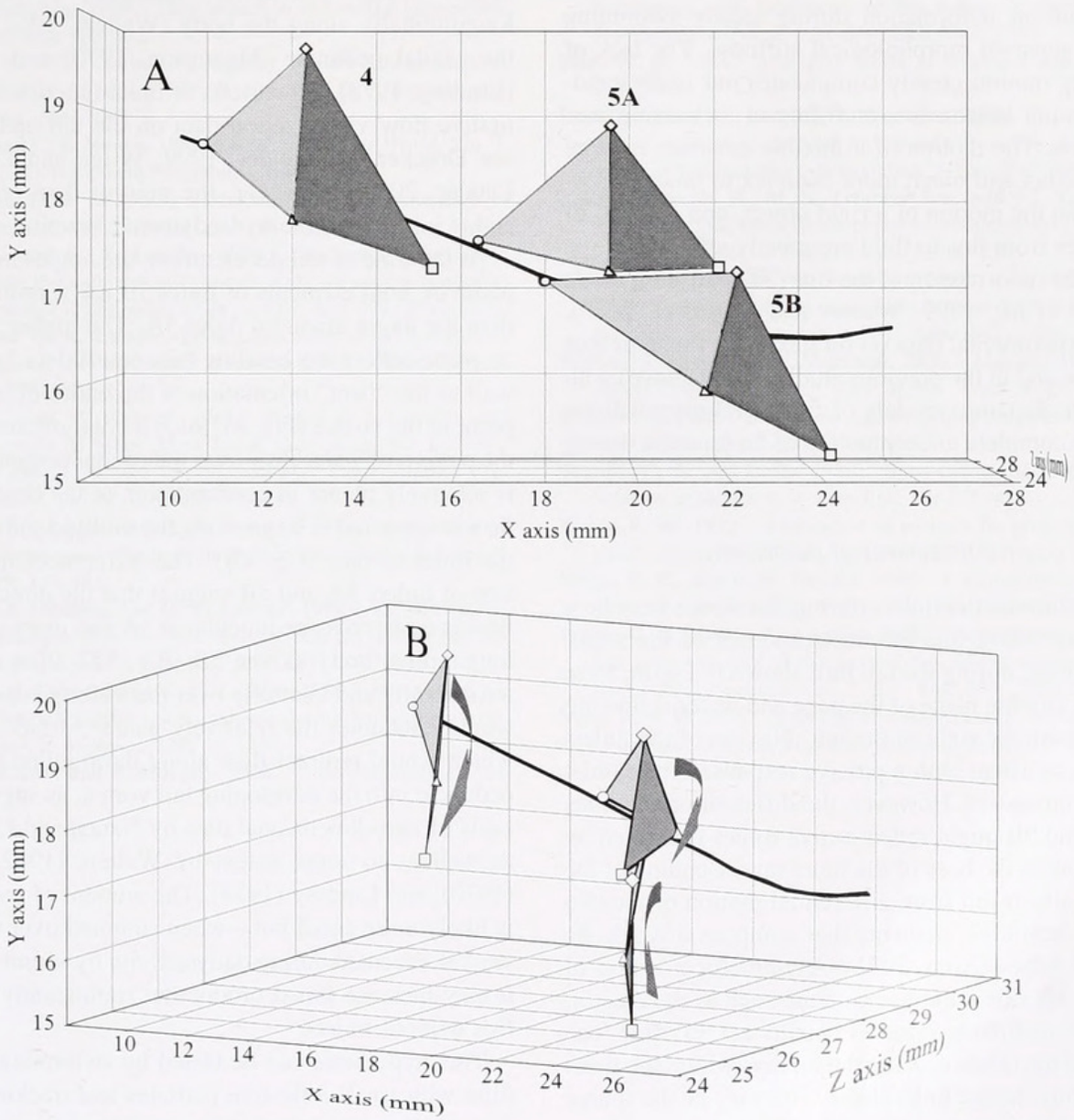

Figure 8. Three-dimensional orientation of finlets 4, 5A, and 5B as the tail is decelerating three-quarters of the way through the stroke. The thick solid line indicates the position of the body midline. The tail is beating into the page. The anterior element of each finlet is shaded light gray, while the posterior element is shaded dark gray. The lateral view (A) is rotated 30° clockwise relative to the *xz* plane in panel B. The arrows in B depict the hypothesized fluid motion based on finlet orientation.

between finlet 5A and 5B, given that mean α values were about 160°. This resulted in a complex, concave structure for the entire fifth finlet for over half of the stroke (see Fig. 8).

Fin deformation during movement has been demonstrated for the pectoral fins of elasmobranchs (Rosenberger and Westneat, 2000; Wilga and Lauder, 2000), chondrosteans (Wilga and Lauder, 1999), and teleosts (Webb, 1973; Geerlink, 1983; Gibb *et al.*, 1994; Lauder and Jayne, 1996; Walker and Westneat, 1997). The caudal fins of elasmobranchs (Ferry and Lauder, 1996), chondrosteans (Wilga and Lauder, 2000) and teleosts (Gibb *et al.*, 1999; Lauder, 2000) are also flexible, to a greater or lesser extent. Although the surface areas of these fins are considerably larger than the finlets studied here, in some cases the finlets also showed significant deformation during steady swimming despite their apparent morphological stiffness. The lack of rigidity during motion greatly complicates our understanding of swimming kinematics, and thus of swimming mechanics, in fish. The motion of a flexible structure is more difficult to predict and much more complex to model mathematically than the motion of a rigid object, and patterns of energy transfer from fins to fluid are greatly affected by the time-dependent deformation of the fins (Triantafyllou *et al.*, 1993; Barrett *et al.*, 1999; Walker and Westneat, 2000). Integrating experimental data on fin flexibility (such as that presented here and in the previous studies listed above) with unsteady hydrodynamic models of fish swimming will result in a more complete understanding of fin function during locomotion.

Active versus passive movement of the finlets

The orientation of the finlets during the stroke may be a combination of active and passive responses of the structure. For example, during the tail beat shown in Figure 8 the tail is beating into the plane of the page and water is flowing over the tail from the right to the left. Flexion of the finlets to the left is consistent with a passive response of the finlet to the water movement. However, the different orientations of finlet 5A and 5B might reflect active forces generated by the musculature at the base of the finlet rays. Bending of the finlets might also result from differential motion of the two bony jointed hemitrich elements that compose a single fin ray in teleost fishes (Arita, 1971). Asymmetrical action of the right and left side finlet musculature such as the erector, depressor, or inclinator muscles would act to slide one hemitrich past the other, causing the fin rays within the finlet to bend and thus change finlet shape. This may be the source of the individual variation seen in the intrafinlet angle of finlet 5A.

The finlet oscillates around its anterior insertion point on the dorsal body midline, thus the angles of the finlets to the xy and yz planes reflect the orientation of the finlets to the body midline. The present data indicate that the maximum xz and yz angles are larger in the posterior finlets and show phased anteroposterior changes to values respectively greater than and less than 90° over a tail stroke. These data agree with previous measurements showing a posterior increase in finlet oscillation amplitude and a posterior phase lag in finlet oscillation (Nauen and Lauder, 2000).

Implications for finlet function

On the basis of the high locomotory performance of scombrid fishes and the position of the finlets immediately anterior to the caudal fin, it has been hypothesized that finlets increase locomotory efficiency by directing flow longitudinally along the body (Walters, 1962), and across the caudal peduncle (Magnuson, 1970) and caudal keels (Lindsey, 1978). Direct tests of finlet function require quantitative flow visualization data on the tail and finlets (*e.g.*, see Drucker and Lauder, 1999; Wilga and Lauder, 1999; Lauder, 2000). However, the present data offer some insights into a possible hydrodynamic function of the finlets.

At the time of tail deceleration, the angles made to the xz plane by both elements of finlet 5B are significantly higher than the angle made by finlet 5A. The higher angles to the xz plane reflect the bending between finlets 5A and 5B, as well as the "bent" orientation of the entire fifth finlet at this point in the stroke (Fig. 8). Such a configuration may affect the pattern of water flow over the caudal peduncle. Finlet 5B is relatively planar in conformation at the time when water flow is expected to be crossing the midline and encountering the finlet surface (Fig. 8B). The differences in the orientation of finlets 5A and 5B suggest that the direction of water flow is more cross-peduncular at 5A and more parallel to the longitudinal body axis at 5B (Fig. 8B). Flow passing posterolaterally and ventrally over the trailing edge of finlet 5A would encounter the relatively planar surface of finlet 5B, which would redirect flow along the midline of the caudal peduncle into the developing tail vortex, as suggested on the basis of two-dimensional data by Nauen and Lauder (2000) as well as to some extent by Walters (1962), Magnuson (1970), and Lindsey (1978). The amount of redirected fluid is likely to be small but—when summed over the many tail strokes executed during daily activity by scombroid fishes—it may increase thrust production significantly relative to a fish without finlets.

This hypothesis can be tested by swimming mackerel in fluid with small reflective particles and tracking the trajectory of the particles as they move past the finlets and the caudal peduncle. Such future experiments with flow visualization will reveal whether the finlets alter the path of water flow in their vicinity and whether that water is directed into the tail vortex, potentially increasing swimming efficiency.

Acknowledgments

The authors thank Cheryl Wilga for assistance with obtaining the mackerel for this study, and Laura Farrell for assistance with data analysis. We also thank Jimmy Liao, Cheryl Wilga, Laura Farrell, Tonia Hsieh, and Ellen Freund for helpful comments during the course of this project. Three reviewers provided useful comments for improving the manuscript. Support was provided by NSF grant 9807021 to GVL.

Literature Cited

Arita, G. S. 1971. A re-examination of the functional morphology of the soft-rays in teleosts. *Copeia* **1971:** 691–697.

Barrett, D. S., M. S. Triantafyllou, D. K. P. Yue, M. A. Grosenbaugh, and M. J. Wolfgang. 1999. Drag reduction in fish-like locomotion. *J. Fluid Mech.* **392:** 183–212.

Beamish, F. W. H. 1978. Swimming capacity. Pp. 101–189 in *Locomotion, Vol. VII, Fish Physiology,* W. S. Hoar and D. J. Randall, eds. Academic Press, New York.

Collette, B. B., and C. E. Nauen. 1983. *Scombrids of the World,* Vol. 2. United Nations Development Programme, FAO, Rome.

Dickinson, M. H. 1996. Unsteady mechanisms of force generation in aquatic and aerial locomotion. *Am. Zool.* **36:** 537–554.

Drucker, E. G., and G. V. Lauder. 1999. Locomotor forces on a swimming fish: three-dimensional vortex wake dynamics quantified with digital particle image velocimetry. *J. Exp. Biol.* **202:** 2393–2412.

Ferry, L. A., and G. V. Lauder. 1996. Heterocercal tail function in leopard sharks: a three-dimensional kinematic analysis of two models. *J. Exp. Biol.* **199:** 2253–2268.

Fierstine, H. L., and V. Walters. 1968. Studies in locomotion and anatomy of scombroid fishes. *Mem. South. Calif. Acad. Sci.* **6:** 1–31.

Geerlink, P. J. 1983. Pectoral fin kinematics of *Coris formosa* (Teleostei, Labridae). *Neth. J. Zool.* **39:** 166–193.

Gibb, A. C., B. C. Jayne, and G. V. Lauder. 1994. Kinematics of pectoral fin locomotion in the bluegill sunfish *Lepomis macrochirus. J. Exp. Biol.* **189:** 133–161.

Gibb, A. C., K. A. Dickson, and G. V. Lauder. 1999. Tail kinematics of the chub mackerel *Scomber japonicus:* testing the homocercal tail model of fish propulsion. *J. Exp. Biol.* **202:** 2433–2447.

Jayne, B. C., A. F. Lozada, and G. V. Lauder. 1996. Function of the dorsal fin in bluegill sunfish: motor patterns during four distinct locomotor behaviors. *J. Morphol.* **228:** 307–326.

Joseph, J., W. Klawe, and P. Murphy. 1988. *Tuna and Billfish: Fish Without a Country.* Inter-American Tropical Tuna Commission, La Jolla, CA.

Lauder, G. V. 2000. Function of the caudal fin during locomotion in fishes: kinematics, flow visualization, and evolutionary patterns. *Am. Zool.* **40:** 101–122.

Lauder, G. V., and B. C. Jayne. 1996. Pectoral fin locomotion in fishes: testing drag-based models using three-dimension kinematics. *Am. Zool.* **36:** 567–581.

Lindsey, C. C. 1978. Form, function, and locomotory habits in fish. Pp. 1–100 in *Locomotion, Vol. VII, Fish Physiology,* W. S. Hoar and D. J. Randall, eds. Academic Press, New York.

Magnuson, J. J. 1970. Hydrostatic equilibrium of *Euthynnus affinis,* a pelagic teleost without a gas bladder. *Copeia* **1970:** 56–85.

Magnuson, J. J. 1978. Locomotion by scombrid fishes: hydromechanics, morphology, and behavior. Pp. 239–313 in *Locomotion, Vol. VII, Fish Physiology,* W. S. Hoar and D. J. Randall, eds. Academic Press, New York.

Nauen, J. C., and G. V. Lauder. 2000. Locomotion in scombrid fishes: morphology and kinematics of the finlets of the chub mackerel *Scomber japonicus. J. Exp. Biol.* **203:** 2247–2259.

Rice, W. R. 1989. Analyzing tables of statistical tests. *Evolution* **43:** 223–225.

Rosenberger, L. J., and M. W. Westneat. 2000. Functional morphology of undulatory pectoral fin locomotion in the stingray *Taeniura lymma* (Chondrichthyes: Dasyatidae). *J. Exp. Biol.* **202:** 3523–3539.

Triantafyllou, G. S., M. S. Triantafyllou, and M. A. Grosenbaugh. 1993. Optimal thrust development in oscillating foils with application to fish propulsion. *J. Fluids Struct.* **7:** 205–224.

Walker, J. A., and M. W. Westneat. 1997. Labriform propulsion in fishes: kinematics of flapping aquatic flight in the bird wrasse *Gomphosus varius* (Labridae). *J. Exp. Biol.* **200:** 1549–1569.

Walker, J. A., and M. W. Westneat. 2000. Mechanical performance of aquatic rowing and flying. *Proc. R. Soc. Lond. B.* **267:** 1875–1881.

Walters, V. 1962. Body form and swimming performance in the scombroid fishes. *Am. Zool.* **2:** 143–149.

Wardle, C. S., and P. He. 1988. Burst swimming speeds of mackerel, *Scomber scombrus* L. *J. Fish Biol.* **32:** 471–478.

Webb, P. W. 1973. Kinematics of pectoral fin propulsion in *Cymatogaster aggregata. J. Exp. Biol.* **59:** 697–710.

Wilga, C. D., and G. V. Lauder. 1999. Locomotion in sturgeon: function of the pectoral fins. *J. Exp. Biol.* **202:** 2413–2432.

Wilga, C. D., and G. V. Lauder. 2000. Three-dimensional kinematics and wake structure of the pectoral fins during locomotion in leopard sharks *Triakis semifasciata. J. Exp. Biol.* **203:** 2261–2278.

Yuen, H. S. H. 1970. Behavior of a skipjack tuna, *Katsuwanus pelamis,* as determined by tracking with ultrasonic devices. *J. Fish. Res. Board Can.* **27:** 2071–2079.